

High-Bandgap Perovskites for Efficient Indoor Light Harvesting

Sergey Shcherbachenko, Oleksandr Astakhov, Zhifa Liu, Li-Chung Kin, Christoph Zahren, Uwe Rau, Thomas Kirchartz, and Tsvetelina Merdzhanova*

The use of metal-halide perovskites in photovoltaic applications has become increasingly attractive due to their low-temperature manufacturing processes and long charge-carrier lifetimes. High-bandgap perovskite solar cells have potential for indoor applications due to their efficient absorption of the spectrum of light-emitting diodes (LEDs). This study investigates the performance of high-bandgap perovskite solar cells under a wide range of lighting conditions, including a commercially available white LED lamp with a 5–40 000 lx illuminance range and a standard 1 sun reference. The performance of $\text{CH}_3\text{NH}_3\text{PbI}_3$ -based perovskite solar cells to $\text{CH}_3\text{NH}_3\text{Pb}(\text{I}_{0.8}\text{Br}_{0.2})_3$ solar cells with varying electron transport layers (ETL), including PCBM, PCBM:CMC, and CMC:ICBA fullerene combinations, is compared. Because the spectral response of perovskite solar cells covers the white LED spectrum very well, the major performance difference is related to the open-circuit voltage and fill factor. The cells with the $\text{CH}_3\text{NH}_3\text{Pb}(\text{I}_{0.8}\text{Br}_{0.2})_3$ absorber layer and the CMC:ICBA ETL demonstrate superior open-circuit voltage and therefore a high efficiency above 29% at 200–500 lx, typical for indoor lighting.

model for the sunlight spectrum.^[8,9] This has led to continuously increasing interest in using halide perovskites for tandem solar cells^[10–12] but also offers opportunities to use the technology for artificial lighting conditions.^[13] As the future of lighting is in white LEDs, and because white LEDs have significantly fewer infrared (IR) and near-infrared spectral components as compared to traditional light bulbs or the solar spectrum, higher-bandgap materials are needed for maximum efficiencies. Depending on the spectrum and color temperature of the LEDs used, the optimum bandgaps for indoor applications range from around 1.7 to 2 eV.^[14] These bandgaps are significantly higher than those of crystalline silicon (1.12 eV) and even those of the halide perovskite solar cells (PSCs) (from 1.5 to 1.6 eV) that show the best efficiencies under 1 Sun illumination.^[15]

Thus, there is a need to explore PSCs with higher bandgaps (>1.7 eV). Perovskite technology provides sufficient flexibility to fabricate these solar cells. However, high-bandgap perovskite cells often suffer from effects such as iodine–bromine segregation,^[16,17] increased bulk recombination,^[18] and a lack of suitable charge transport materials with good energy-level matching at interfaces.^[19–22]


Artificial indoor LED lighting is characterized by a narrower spectrum and significantly reduced intensity with respect to the 1 Sun standard test conditions. A drastic decrease in intensity leads to an efficiency reduction.^[23–26] At low illumination, even a low current through the parasitic shunt resistance gains

1. Introduction

Low-temperature manufacturing processes using inexpensive solution-processing methods,^[1] combined with exceptionally long charge-carrier lifetimes,^[2–4] have made metal-halide perovskites attractive materials for photovoltaic applications.^[5] Due to intensive research efforts, efficiencies have increased to 25.7%^[6] over the course of 10 years, since the first cells surpassed the 10% mark in 2012.^[7] A peculiar feature of halide perovskites is that they achieve their best efficiencies for bandgaps that are slightly higher than ideal from the perspective of the Shockley–Queisser

S. Shcherbachenko, O. Astakhov, Z. Liu, L.-C. Kin, C. Zahren, U. Rau, T. Kirchartz, T. Merdzhanova
IEK-5 Photovoltaik
Forschungszentrum Jülich GmbH
Wilhelm-Johnen Straße, 52425 Jülich, Germany
E-mail: t.merdzhanova@fz-juelich.de

S. Shcherbachenko, U. Rau
Jülich Aachen Research Alliance
JARA-Energy and Faculty of Electrical Engineering and Information Technology
RWTH Aachen University
Schinkelstr. 2, 52062 Aachen, Germany

 The ORCID identification number(s) for the author(s) of this article can be found under <https://doi.org/10.1002/aesr.202400032>.

© 2024 The Authors. Advanced Energy and Sustainability Research published by Wiley-VCH GmbH. This is an open access article under the terms of the Creative Commons Attribution License, which permits use, distribution and reproduction in any medium, provided the original work is properly cited.

DOI: 10.1002/aesr.202400032

L.-C. Kin
IEK-9
Grundlagen der Elektrochemie
Forschungszentrum Jülich
52425 Jülich, Germany

T. Kirchartz
Faculty of Engineering and CENIDE
University of Duisburg-Essen
Carl-Benz-Str. 199, 47057 Duisburg, Germany

importance and reduces solar cell efficiency.^[23,25–27] PSCs, however, show potential for a high shunt resistance R_{SH} ,^[13,28–31] making them suitable for low-illumination applications. In addition, Kin et al. demonstrated the exceptional efficiency of these cells when integrated with sodium-ion batteries under indoor illumination.^[32]

Spectrum narrowing can be very beneficial for solar cell efficiency.^[13,14,23,28–31,33] The emission spectra of indoor LED light sources are often very efficiently absorbed by the PSCs and, therefore, the losses in short-circuit current density J_{SC} are low. Therefore, most optimization efforts must focus on the V_{OC} and filler factor (FF) losses under indoor illumination. In this work, we focus on maximizing the V_{OC} of the PSCs for indoor applications.

To explore this optimization direction, we studied the light intensity-dependent performance of $\text{CH}_3\text{NH}_3\text{Pb}(\text{I},\text{Br})_3$ solar cells with different I-to-Br ratios that have fairly high open-circuit voltages between 1.19 and 1.33 V for bandgaps between 1.6 and 1.72 eV. We compare two absorber compositions with (i) pure iodine ($\text{CH}_3\text{NH}_3\text{PbI}_3$, $E_g = 1.6$ eV) and with 20% Br ($\text{CH}_3\text{NH}_3\text{Pb}(\text{I}_{0.8}\text{Br}_{0.2})_3$, $E_g = 1.72$ eV). The absorbers were grown using PbAc_2 -based precursors, as previously described by Liu et al.^[19,34] The solar cells are based on a pin-type geometry, as shown in **Figure 1**, where the perovskite layer is sandwiched between an ITO/PTAA anode on the illuminated front side of the device and a fullerene/bathocuproine (BCP)/Ag cathode on the back. The fullerenes used include [6,6]-phenyl- C_{61} -butyric acid methyl ester (PCBM), which is used for Br-free cells, and PCBM, PCBM:CMC, and CMC:ICBA for Br-containing cells. Here, ICBA is the indene C_{60} bisadduct known for its significantly lower electron affinity^[35,36] as compared to PCBM or even C_{60} , whereas CMC is C_{60} -fused Nmethylpyrrolidinem C_{12} phenyl. The use of lower-electron-affinity fullerenes, such as ICBA and CMC, is crucial for improving the energy-level alignment to higher-bandgap perovskites and minimizing losses due to interfacial recombination,

which are known to deteriorate the performance of high-bandgap PSCs. Both absorber compositions have been previously shown to enable high open-circuit voltages,^[19,34] due to their very high bulk lifetimes, negligible recombination at the perovskite–PTAA interface, and reduced recombination at the perovskite–ETL interface. However, it has already been clear from previous work that the perovskite–ETL interface is the performance-limiting interface that causes significant additional recombination in the device compared to perovskite films on glass or on PTAA.^[2,37]

In this work, we vary the electron transport layer (ETL) between the combinations of PCBM, CMC, and ICBA fullerenes and study the performance of these cells under LED illumination with varied irradiance and under 1 Sun illumination. Following our previous work^[19,34] dedicated to achieving high 1 Sun V_{OC} in these cells, we now focus on performance under LED light and discuss trends in irradiance dependence that affect the indoor light harvesting performance.

2. Results and Discussion

Four types of PSCs were investigated in this work: high-bandgap $\text{CH}_3\text{NH}_3\text{Pb}(\text{I}_{0.8}\text{Br}_{0.2})_3$ cells with CMC:ICBA, PCBM, and PCBM:CMC ETLs and a reference $\text{CH}_3\text{NH}_3\text{PbI}_3$ cell with a PCBM ETL. The fabrication procedure for the $\text{CH}_3\text{NH}_3\text{PbI}_3$ cell was discussed in ref. [34], while the detailed fabrication procedure for the $\text{CH}_3\text{NH}_3\text{Pb}(\text{I}_{0.8}\text{Br}_{0.2})_3$ cells was presented in ref. [19]. **Figure 2** presents the J – V curves of these solar cells under 1 Sun and 175 lx LED illumination (lowest measured point close to the 200–500 lx region).

Four types of PSCs were investigated in this work: high-bandgap $\text{CH}_3\text{NH}_3\text{Pb}(\text{I}_{0.8}\text{Br}_{0.2})_3$ cells with CMC:ICBA, PCBM, and PCBM:CMC ETLs and a reference $\text{CH}_3\text{NH}_3\text{PbI}_3$ cell with a PCBM electron transport layer. The fabrication procedure for the $\text{CH}_3\text{NH}_3\text{PbI}_3$ cell was discussed in ref. [34], while the detailed fabrication procedure for the $\text{CH}_3\text{NH}_3\text{Pb}(\text{I}_{0.8}\text{Br}_{0.2})_3$ cells was presented in ref. [19]. **Figure 2** presents the J – V curves of these solar cells under 1 Sun and 175 lx LED illumination (lowest measured point close to the 200–500 lx region). **Table 1** presents the corresponding solar cell parameters: open-circuit voltage (V_{OC}), short-circuit current (I_{SC}), short-circuit current density (J_{SC}), short-circuit current density calculated from EQE ($J_{SC, EQE}$), device area (A), FF, power at maximum power point (P_{MPP}), and efficiency (η). $J_{SC, EQE}$ was calculated for two cells (with $\text{CH}_3\text{NH}_3\text{Pb}(\text{I}_{0.8}\text{Br}_{0.2})_3$ absorber and CMC:ICBA electron transport layers and with $\text{CH}_3\text{NH}_3\text{PbI}_3$ absorber and PCBM electron transport layers) using EQE measured for the cells with the same composition.

The solar cell with the $\text{CH}_3\text{NH}_3\text{PbI}_3$ absorber layer has a bandgap of 1.6 eV and consequently lower V_{OC} of 0.86 V at 175 lx LED and 1.18 V at 1 Sun. PSCs with the $\text{CH}_3\text{NH}_3\text{Pb}(\text{I}_{0.8}\text{Br}_{0.2})_3$ (1.72 eV bandgap) absorber layer show open-circuit voltages in the range of 1.24–1.3 V at 1 Sun and around 1.02–1.06 V at 175 lx LED illumination. Among them, the cell with a blend of CMC and ICBA used as an ETL has the highest V_{OC} of 1.29 V at 1 Sun and 1.06 V at 175 lx LED illumination. From the low illumination current–voltage curves (**Figure 2b**), one can see that the shunt resistance of these cells is extremely high, ensuring a stable and high FF (above 75% for CMC:ICBA ETL cells) even at 175 lx.

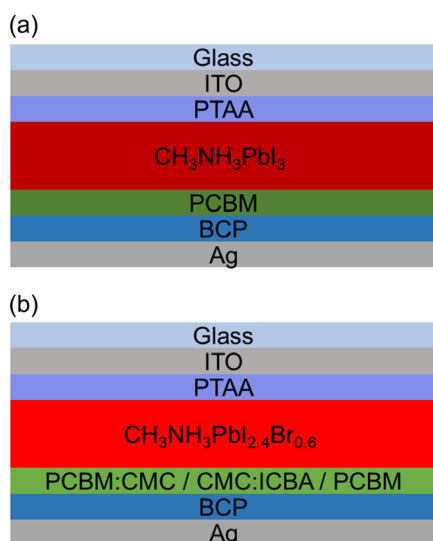


Figure 1. Schematic of the layer stacks of the PSCs used in this study. The solar cell with the $\text{CH}_3\text{NH}_3\text{PbI}_3$ absorber layer a) has a PCBM ETL. Solar cells with the $\text{CH}_3\text{NH}_3\text{Pb}(\text{I}_{0.8}\text{Br}_{0.2})_3$ absorber layer b) have ETLs consisting of different combinations of the fullerenes PCBM, CMC, and ICBA.

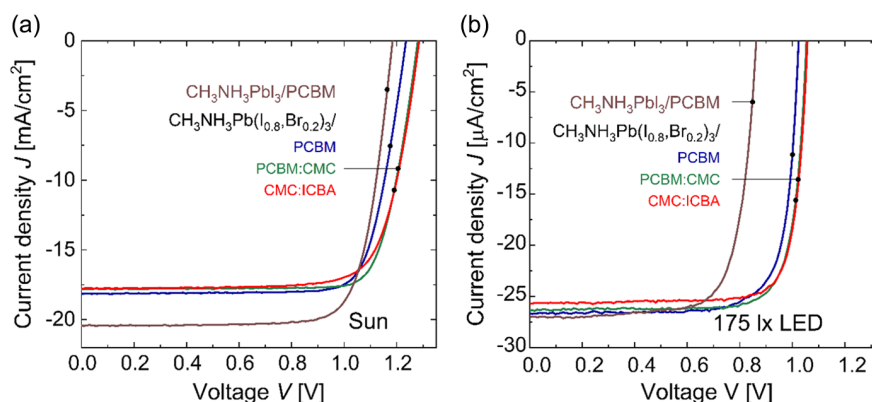


Figure 2. J - V characteristics of PSCs used in this study under 1 Sun a) and 175 lx LED light b). The solar cell with the $\text{CH}_3\text{NH}_3\text{PbI}_3$ absorber layer has a PCBM ETL. Three solar cells with a $\text{CH}_3\text{NH}_3\text{Pb}(\text{I}_{0.8}\text{Br}_{0.2})_3$ absorber layer have PCBM, PCBM:CMC, and CMC:ICBA fullerene blends as ETLs.

Table 1. Parameters of PSCs used in this study under room conditions (175 lx LED) and under 1 sun.

Source	$\text{CH}_3\text{NH}_3\text{Pb}(\text{I}_{0.8}\text{Br}_{0.2})_3$		$\text{CH}_3\text{NH}_3\text{Pb}(\text{I}_{0.8}\text{Br}_{0.2})_3$		$\text{CH}_3\text{NH}_3\text{Pb}(\text{I}_{0.8}\text{Br}_{0.2})_3$		$\text{CH}_3\text{NH}_3\text{PbI}_3$	
	CMC:ICBA		PCBM:CMC		PCBM		PCBM	
	LED	Sun	LED	Sun	LED	Sun	LED	Sun
V_{OC} [V]	1.06	1.29	1.05	1.28	1.02	1.24	0.86	1.18
I_{SC} [mA]	0.0041	2.85	0.0042	2.85	0.0043	2.90	0.0043	3.27
J_{SC} [mA cm^{-2}]	0.0257	17.79	0.0264	17.82	0.0267	18.15	0.0270	20.43
$J_{\text{SC, EQE}}$ [mA cm^{-2}]	0.02560	18.68	—	—	—	—	0.0288	20.04
A [cm^2]	0.16	0.16	0.16	0.16	0.16	0.16	0.16	0.16
FF [%]	80.82	75.87	79.86	79.58	77.97	78.22	74.11	77.65
P_{MPP} [mW cm^{-2}]	0.0220	17.30	0.0222	18.20	0.0213	17.50	0.0173	18.80
η [%]	29.36	17.30	29.62	18.20	28.42	17.50	23.09	18.80

Although in this work $\text{CH}_3\text{NH}_3\text{PbI}_3$ cells show considerably lower voltages than $\text{CH}_3\text{NH}_3\text{Pb}(\text{I}_{0.8}\text{Br}_{0.2})_3$ cells, our previous work on this cell reported an even higher V_{OC} of 1.26 V after light soaking.^[34]

Figure 3a,b presents the open-circuit voltage V_{OC} and FF dependences on the light source power density for the solar cells used in this study.

The measurement results under standard test conditions, 1 Sun illumination, are highlighted in yellow. The region of typical indoor illumination (200–500 lx) is marked by a blue vertical bar in Figure 3. The LED power density range of all points tested is 0.002–15.5 mW cm^{-2} and corresponds to ≈ 5 –40 000 lx.

For all PSCs, a smooth quasilinear dependence of V_{OC} on power density is observed on the semilogarithmic scale. The cells closely follow the classical diode dependence of V_{OC} on J_{SC} ^[38,39]

$$V_{\text{OC}} = \frac{n_{\text{id}} k T}{q} \ln \left(\frac{J_{\text{SC}}}{J_0} \right) \quad (1)$$

Using Equation (1), the ideality factors of these cells were determined from the data in Figure 3a. The dashed lines representing the slopes for $n_{\text{id}} = 1$ and $n_{\text{id}} = 2$ are plotted for reference. The solar cells with $\text{CH}_3\text{NH}_3\text{Pb}(\text{I}_{0.8}\text{Br}_{0.2})_3$ showed ideality factors between 1.6 and 1.63, while the lower-bandgap $\text{CH}_3\text{NH}_3\text{PbI}_3$ cell

showed an ideality factor of 2.25. A lower ideality factor corresponds to a flatter slope and a higher V_{OC} at low irradiance. The higher-bandgap cells in this study showed considerably more stable V_{OC} over the entire illuminance range compared to the cell with a lower bandgap. The V_{OC} decreases by ≈ 0.38 V in high-bandgap cells as the illuminance decreases from 40 000 to 5 lx, while a larger V_{OC} reduction of 0.49 V is observed in the lower-bandgap solar cell. Simultaneously, similar V_{OC} values are observed for 1 Sun illumination and high-power LED illumination. Higher initial voltages of the $\text{CH}_3\text{NH}_3\text{Pb}(\text{I}_{0.8}\text{Br}_{0.2})_3$ cells (Figure 3a) combined with lower V_{OC} drops result in higher V_{OC} values at low irradiance as compared to a PSC with a $\text{CH}_3\text{NH}_3\text{PbI}_3$ absorber layer (brown squares in Figure 3a). Under indoor illumination conditions, the $\text{CH}_3\text{NH}_3\text{Pb}(\text{I}_{0.8}\text{Br}_{0.2})_3$ cell with the CMC:ICBA ETL (red diamonds) shows a V_{OC} above 1.05 V and we observe a strong difference between low-bandgap and high-bandgap solar cells.

A special note can be given to the V_{OC} of the CMC:ICBA cell. The V_{OC} of this device remained above 1.1 V under LED illumination with an irradiance of 0.3 mW cm^{-2} and increased up to 1.3 V at 15.5 mW cm^{-2} . Under 1 Sun illumination (100 mW cm^{-2} AM1.5), the cell showed a V_{OC} of 1.29 V. These results are in agreement with those of our previous work,^[19] where the highest voltage was achieved by a cell with the same structure.

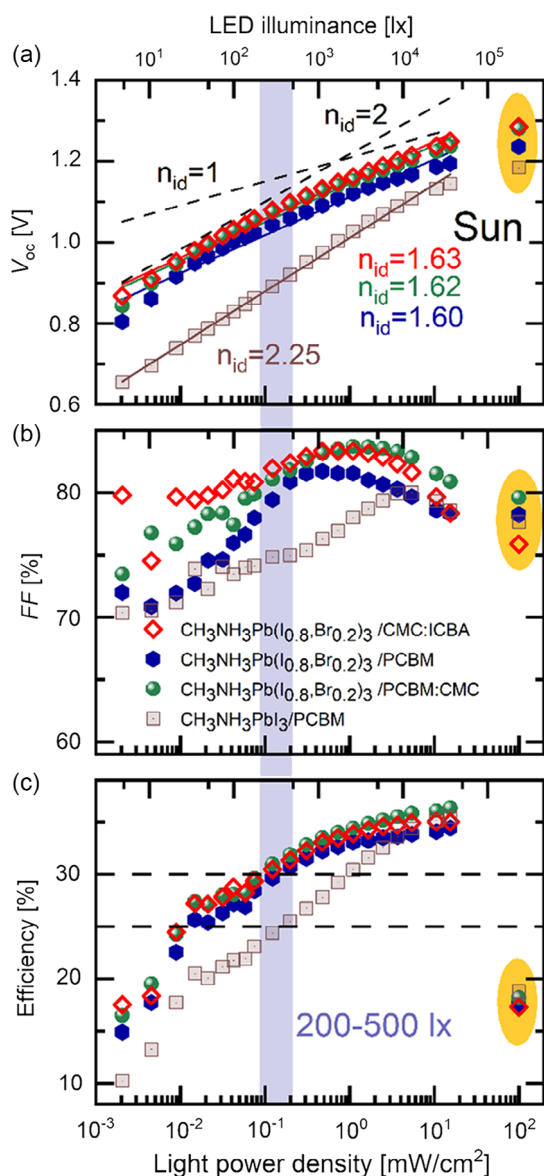


Figure 3. Open-circuit voltage, a) V_{OC} , b) FF , and power conversion efficiency c) as a function of the power density of the LED and reference values measured under 1 Sun illumination (yellow area) for different PSCs. The top x-axis corresponds to illuminance values in lux calculated for the LED spectrum (1 Sun AM1.5 spectrum corresponds to 100 mW cm^{-2} and $\approx 10^5 \text{ lx}$, and the position of the points is defined by the power density value). The region marked with blue rectangle represents standard office room conditions (200–500 lx). The ideality factors of the three wide-bandgap perovskites are labeled in (a) in their corresponding colors.

The FF of a solar cell J – V curve is defined as $FF = V_{MPP} J_{MPP} / (V_{OC} J_{SC})$, where V_{MPP} and J_{MPP} are the voltage and current density at the maximum power point. It depends on the ideality factor n_{id} , as well as the shunt and series resistances R_{SH} and R_S , and is positively correlated with the open-circuit voltage (V_{OC}). Following the approach,^[40] for the case of an ideal diode with infinitely large shunt resistance and zero series resistance, the FF dependence on V_{OC} can be approximated with

$$FF_0 = \frac{v_{oc} - \ln(v_{oc} + 0.72)}{v_{oc} + 1} \quad (2)$$

where

$$v_{oc} = \frac{V_{OC}}{n_{id} kT/q} \quad (3)$$

As the V_{OC} increases with the illumination intensity (Figure 3a), an increase in FF is observed (Figure 3b) for all PSCs. Additionally, the FF strongly depends on the shunt and series resistances of the solar cell.^[41,42] The effect of the shunt resistance is more pronounced under low LED light power density, whereas the series resistance is important at high illumination intensities, where the current density at the maximum power point increases.^[26] The series resistance of the cells leads to a drop in the FF observed under LED irradiance above 10 000 lx. At the same time, PSCs can have a remarkably high shunt resistance,^[13,28–31] which was also the case for the presented PSCs (Figure 3), demonstrating a very stable FF at low illumination intensities.

Figure 3c presents the dependence of the cell efficiency on the LED power density and includes the reference values under 1 Sun irradiance represented by the points in the yellow area. Comparing the performances of PSCs under 1 Sun and under high power densities of white LED, higher power conversion efficiencies (34–36.5%) were observed under LED light as compared to 17–19% under 1 Sun. This is related to the high bandgap of the perovskite absorbers and, therefore, a much better match of their EQE to the LED spectrum as compared to the Sun spectrum (Figure 6). In the case of LED light, both perovskite absorber materials show external quantum efficiencies above 80% over the entire range of the LED spectrum, except for the minor fraction of the IR region 740–800 nm, where the LED emission is weak. Therefore, under LED light, both absorbers exhibited very similar J_{SC} values (Table 1). At the same time, the wider bandgap of $\text{CH}_3\text{NH}_3\text{Pb}(\text{I}_{0.8}\text{Br}_{0.2})_3$ provides a noticeably higher V_{OC} , likely due to the reduction in thermalization losses even under LED light. The thermalization loss refers to the energy loss during vibrational (thermal) relaxation of an excited electron to the lowest available level of the conduction band.^[43] A high bandgap reduces the amount of energy that an electron releases during such a process and results in a considerably higher V_{OC} and efficiency of the cells with the $\text{CH}_3\text{NH}_3\text{Pb}(\text{I}_{0.8}\text{Br}_{0.2})_3$ base layer. The cell with the highest V_{OC} has a CMC:ICBA ETL layer and shows an efficiency of above 29% in office-lighting conditions (200–500 lux), 28.5% efficiency under a lower illuminance of 100 lx, while a maximum efficiency of 35.5% is observed under $\approx 4000 \text{ lx}$ of LED light.

Figure 4a presents the dependence of the shunt resistance (R_{SH}) on the LED light power density.

The resistance was determined from the slope of the corresponding J – V curve at $V = 0$, so any linear term in the dependence of current on voltage was perceived as shunt. As a result, we observe the real shunt resistance in parallel with a “photo-shunt,”^[44,45] which shows a linear dependence on the light power density. As these two effects act in parallel, the lower of the two resistances will dominate. At high LED power density, the photo-shunt resistance decreases, and the overall resistance shows a linear dependence on light intensity. Moving to low irradiance,

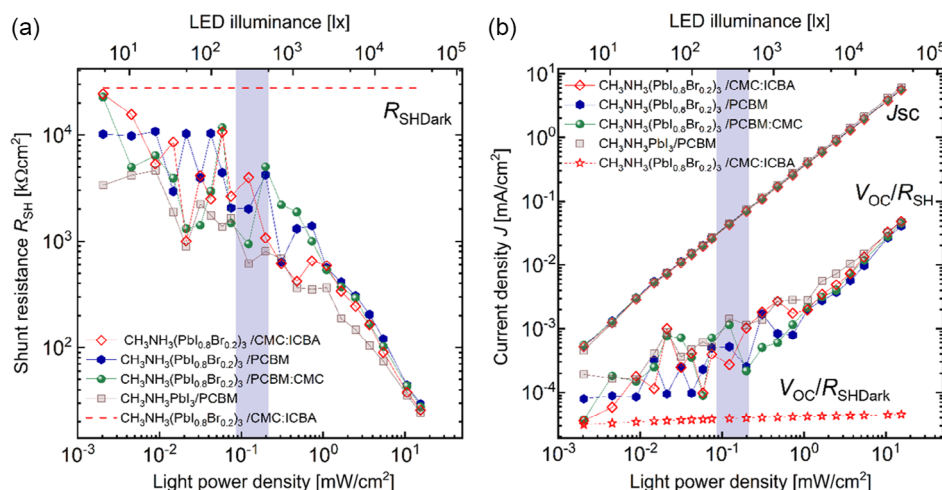


Figure 4. a) Dependence of the shunt resistance R_{SH} on LED light power density for different PSCs. b) Dependence of the short-circuit current density and the estimated shunt current (calculated as V_{OC}/R_{SH}) on LED light power density. The top x-axis corresponds to illuminance values in lux. The values of R_{SH} and V_{OC}/R_{SH} with R_{SH} calculated from the dark $J-V$ (R_{SHDark}) are presented for one cell as a reference in both plots (red dashed line(a) and red stars(b)). The region marked with blue rectangle represents standard office room conditions (200–500 lx).

the photoshunt resistance increases, while the total shunt resistance saturates around the value determined from the dark $J-V$ curve ($\approx 20\,000\text{ k}\Omega\text{cm}^2$). In the region corresponding to room conditions (marked with blue rectangle), PSCs show shunt resistances above $1000\text{ k}\Omega\text{cm}^2$.

In the single-diode model with shunt resistance, a correction term V_{OC}/R_{SH} appears (Equation (4)), which leads to the reduction of V_{OC} .

$$V_{OC} = \frac{n_{id}kT}{q} \ln \left(\frac{J_{SC} - V_{OC}/R_{SH}}{J_0} \right) \quad (4)$$

The value of this correction term V_{OC}/R_{SH} is compared to the magnitude of J_{SC} in Figure 4b for the studied LED power density range. As the J_{SC} is at least one (almost two) order of magnitude higher than V_{OC}/R_{SH} at irradiances corresponding to room conditions and above, the shunt resistance has minor influence on the V_{OC} in the perovskite cells presented in this study.

The dependencies presented in Figure 3 fully describe the performance of the studied cells, but for potential practical indoor applications of PSCs, it is more instructive to plot the dependence of the PSC output power density on the LED lighting power density on a linear scale as it is presented in Figure 5. For example, the PSCs used in this study can provide a power density of $38\text{ }\mu\text{W cm}^{-2}$ under LED illumination with 0.12 mW cm^{-2} power density. Additionally, a power density of $20\text{--}60\text{ }\mu\text{W cm}^{-2}$ can be expected in suggested room lighting conditions (white LED illumination of 200–500 lx). This value can be used to estimate the solar cell (or module) area required to supply power to certain electronic applications in an indoor setting.

Comparing the results of this work with the literature data,^[13,28–31] we conclude that the PSC with the $\text{CH}_3\text{NH}_3\text{Pb}(\text{I}_{0.8}\text{Br}_{0.2})_3$ bandgap and CMC:ICBA has exceptionally good performance under white LED illumination of 100–1000 lx (Table 2) and stays on par with or exceeds the best values reported in the

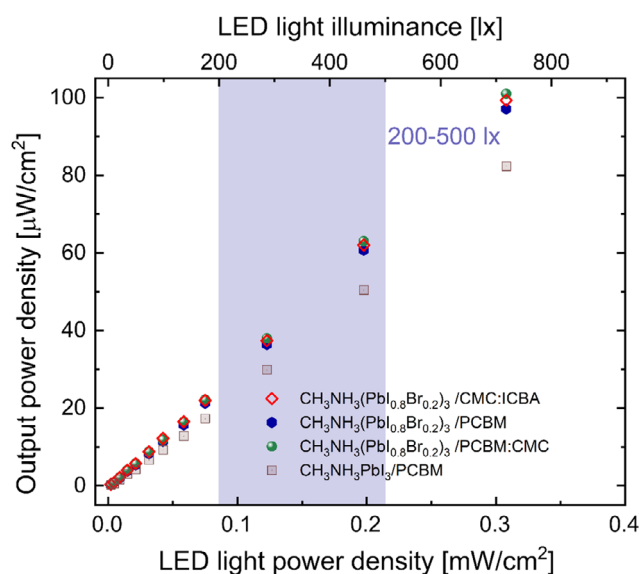


Figure 5. Dependence of the output power density of PSCs on the power density delivered by the LED light source. The blue region represents standard office room conditions (200–500 lx).

literature, especially relevant for indoor application range of 200–500 lx.^[13,28–31]

3. Conclusion

We studied the potential of high-bandgap PSCs for indoor applications under LED light. The quantum efficiency of PSCs closely matches that of common LED lights, thereby providing efficient absorption. Therefore, further performance improvement efforts must focus on V_{OC} and FF under low-intensity LED light. To

Table 2. Comparison of the performance between the $\text{CH}_3\text{NH}_3\text{Pb}(\text{I}_{0.8}\text{Br}_{0.2})_3$ cell with CMC:ICBA electron transport layer and other reported perovskite cells in similar conditions.

Irradiance	Illuminance of LED	Cell efficiency [%]	References	This work [%]
0.3 mW cm^{-2}	800 lx	40.1	[13]	32.3
–	1000 lx	36.2	[29]	32.6
0.3 mW cm^{-2}	1000 lx	27.4	[31]	32.6
–	400 lx	26.9	[28]	30.9
–	200 lx	25	[30]	29.4
–	100 lx	22.5	[31]	28.5

achieve a high V_{OC} under low-light conditions, we studied PSCs with a wide-bandgap $\text{CH}_3\text{NH}_3\text{Pb}(\text{I}_{0.8}\text{Br}_{0.2})_3$ absorber layer ($E_g = 1.72 \text{ eV}$) in combination with three ETLs (PCBM) and two PCBM:CMC and CMC:ICBA fullerene combinations. The high-bandgap cells were compared to a reference cell with a $\text{CH}_3\text{NH}_3\text{PbI}_3$ absorber layer ($E_g = 1.6 \text{ eV}$) and a PCBM ETL. The wide-bandgap $\text{CH}_3\text{NH}_3\text{Pb}(\text{I}_{0.8}\text{Br}_{0.2})_3$ solar cells showed 1 Sun V_{OC} of 1.24–1.29 V, while $\text{CH}_3\text{NH}_3\text{PbI}_3$ solar cell showed lower 1 Sun V_{OC} of 1.18 V.

All solar cells were tested under LED illumination with illuminance ranging from 5 to 40 000 lx. The wide-bandgap $\text{CH}_3\text{NH}_3\text{Pb}(\text{I}_{0.8}\text{Br}_{0.2})_3$ cells reveal persistent V_{OC} with flat dependence on irradiance corresponding to an ideality factor of ≈ 1.6 and a V_{OC} of 1 V around 200–500 lx. The reference $\text{CH}_3\text{NH}_3\text{PbI}_3$ cell showed a V_{OC} of 0.86 V at 200–500 lx and a steeper V_{OC} dependence on irradiance with ideality factor of ≈ 2.25 .

All studied cells show high FF under low light due to high shunt resistance above $1000 \text{ k}\Omega\text{cm}^2$. However, the wide-bandgap cells demonstrate a higher FF in most cases with FF of $\approx 80\%$ at 200–500 lx. With similar currents but higher V_{OC} and FF values, the wide-bandgap cells show a significant gain in efficiency as compared to the reference $\text{CH}_3\text{NH}_3\text{PbI}_3$ cell.

Efficiencies of 30–32% are observed in the range of 200–500 lx, dropping to 28.5% at 100 lx for the highest V_{OC} cell with a $\text{CH}_3\text{NH}_3\text{Pb}(\text{I}_{0.8}\text{Br}_{0.2})_3$ absorber layer and a CMC:ICBA electron transport layer. These results agree with the performance of the best reported PSCs under white LED illumination^[13,28–31] and demonstrate the high potential of the PCSs for indoor light harvesting. To facilitate the practical use of these devices, we present the dependence of the output power density on LED light power density. We expect that light harvesters based on PCSs will deliver $\approx 20\text{--}60 \mu\text{W cm}^{-2}$ under realistic room lighting conditions.

4. Experimental Section

While standards for low-light LED characterization of solar cells are yet to be developed, there are several light conditions that one can usually see in the literature. The region of 300–500 lx of “white LED” is a standard for office work.^[46] Jobs involving small objects require higher illuminance, whereas offices and nonworking areas can have lower average illumination levels.^[47] Consequently, the test conditions used in the literature varied between 100 and 1000 lx. At the same time, the standards for illuminance are defined for working desks, while light-harvesting devices can be installed anywhere in a room. Hence, a real room can provide an even wider range of conditions including shaded areas with extremely low illumination. For example, the DIN EN 12464-1 standard sets minimal

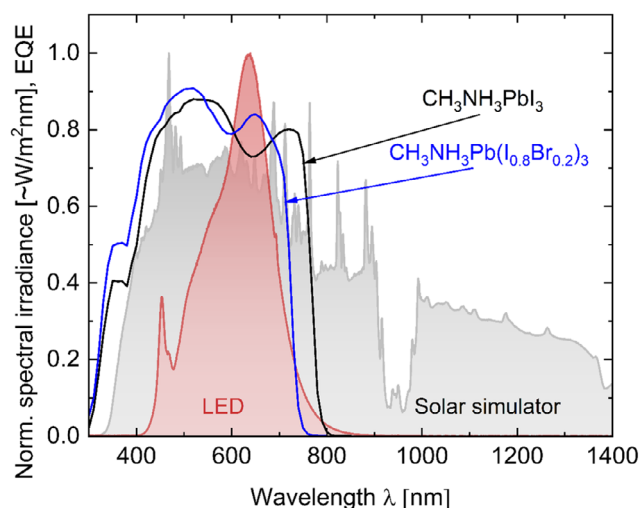


Figure 6. Normalized spectral irradiance of the solar simulator (gray area) and the white LED lamp (red area) used in this study. The spectra are compared with the external quantum efficiencies of $\text{CH}_3\text{NH}_3\text{PbI}_3$ (black line) and $\text{CH}_3\text{NH}_3\text{Pb}(\text{I}_{0.8}\text{Br}_{0.2})_3$ (blue line) PSCs.

illuminance of 30–50 lx on ceilings and 50–75 lx on walls. This article addresses the performance of PSCs in a wide range of possible conditions from 5 to 40 000 lx, while extending the standard range of office conditions to the 200–500 lx range.

Characterization of solar cells under 1 Sun illumination (AM1.5 spectrum, 100 mW cm^{-2}) was performed using a class-A sun simulator. A commercially available white LED lamp (Cree XLamp CXA3050 LED with a color temperature of 3000 K) in combination with a neutral-density OD1 filter served as the light source for indoor illumination tests. The standard test procedure involves measurements at different LED light powers, progressing from the lowest to highest power. We chose this progression to avoid possible light soaking^[48,49] and the influence of the measurements performed at high intensity on the measurements at low intensity. For current–voltage characterization, both forward and backward voltage sweeps were done with 0.01 V steps, 20 ms delay, and LED light remaining between the sweeps and changes in irradiance. All presented results corresponded to the down-sweep ($V_{\text{OC}} \rightarrow J_{\text{SC}}$) direction.

The power output of the LED lamp was controlled by the LED lamp current. Solar and LED spectra were measured with a compact array spectrometer from “Instrument Systems” at a predefined set of currents. One of the resulting normalized spectra is presented in Figure 6. From these measurements, the dependence of the irradiance E_e on the LED current was determined and used to interpolate points that were not measured. The spectral response of the neutral-density filter was calculated separately and multiplied by the measured LED spectrum. The illuminance E_v of the LED lamp was calculated from the spectrum of the LED lamp with a filter at 210 mA LED current and was derived as $E_v(x) = E_v(210 \text{ mA}) * P_d(x)/P_d(210)$, where E_v is illuminance of the LED lamp and P_d is power density for all other measurement points. Detailed description of LED light characterization and calculation of illuminance is presented in the Supporting Information.

Supporting Information

Supporting Information is available from the Wiley Online Library or from the author.

Acknowledgements

The authors would like to thank Benjamin Klingebiel for his help with the measurement box operation. The authors acknowledge the HITEC

fellowship program for funding. This work was supported by the European Union's Horizon Europe as a part of SUPERVAL project (The Sustainable Photo-Electrochemical VALorization of flue gases) (grant agreement no. 101115456).

Conflict of Interest

The authors declare no conflict of interest.

Data Availability Statement

The data that support the findings of this study are available from the corresponding author upon reasonable request.

Keywords

bandgap matching, internet of things, LED illuminations, perovskite solar cells

Received: January 31, 2024

Published online: February 9, 2024

- [1] Y. Rong, Y. Hu, A. Mei, H. Tan, M. I. Saidaminov, S. I. Seok, M. D. McGehee, E. H. Sargent, H. Han, *Science* **2018**, 361, eaat8235.
- [2] L. Krückemeier, B. Krogmeier, Z. Liu, U. Rau, T. Kirchartz, *Adv. Energy Mater.* **2021**, 11, 2003489.
- [3] D. W. deQuilettes, S. Koch, S. Burke, R. K. Paranj, A. J. Shropshire, M. E. Ziffer, D. S. Ginger, *ACS Energy Lett.* **2016**, 1, 438.
- [4] W. Tress, *Adv. Energy Mater.* **2017**, 7, 1602358.
- [5] A. K. Jena, A. Kulkarni, T. Miyasaka, *Chem. Rev.* **2019**, 119, 3036.
- [6] O. Almora, D. Baran, G. C. Bazan, C. Berger, C. I. Cabrera, K. R. Catchpole, S. Erten-Ela, F. Guo, J. Hauch, A. W. Y. Ho-Baillie, T. J. Jacobsson, R. A. J. Janssen, T. Kirchartz, N. Kopidakis, Y. Li, M. A. Loi, R. R. Lunt, X. Mathew, M. D. McGehee, J. Min, D. B. Mitzi, M. K. Nazeeruddin, J. Nelson, A. F. Nogueira, U. W. Paetzold, N.-G. Park, B. P. , U. Rau, H. J. Snaith, E. Unger, et al. *Adv. Energy Mater.* **2021**, 11, 2102526.
- [7] M. M. Lee, J. Teuscher, T. Miyasaka, T. N. Murakami, H. J. Snaith, *Science* **2012**, 338, 643.
- [8] W. Shockley, H. J. Queisser, *J. Appl. Phys* **1961**, 32, 510.
- [9] L. Krückemeier, U. Rau, M. Stolterfoht, T. Kirchartz, *Adv. Energy Mater.* **2020**, 10, 1902573.
- [10] K. O. Brinkmann, T. Becker, F. Zimmermann, C. Kreusel, T. Gahlmann, M. Theisen, T. Haeger, S. Olthof, C. Tücmantel, M. Günster, T. Maschwitz, F. Göbelsmann, C. Koch, D. Hertel, P. Caprioglio, F. Peña-Camargo, L. Perdigón-Toro, A. Al-Ashouri, L. Merten, A. Hinderhofer, L. Gomell, S. Zhang, F. Schreiber, S. Albrecht, K. Meerholz, D. Neher, M. Stolterfoht, T. Riedl, *Nature* **2022**, 604, 280.
- [11] A. Al-Ashouri, E. Köhnen, B. Li, A. Magomedov, H. Hempel, P. Caprioglio, J. A. Márquez, A. B. Morales Vilches, E. Kasparavicius, J. A. Smith, N. Phung, D. Menzel, M. Grischek, L. Kegelmann, D. Skroblin, C. Gollwitzer, T. Malinauskas, M. Jošt, G. Matič, B. Rech, R. Schlattmann, M. Topič, L. Korte, A. Abate, B. Stannowski, D. Neher, M. Stolterfoht, T. Unold, V. Getautis, S. Albrecht, *Science* **2020**, 370, 1300.
- [12] M. Jošt, L. Kegelmann, L. Korte, S. Albrecht, *Adv. Energy Mater.* **2020**, 10, 1904102.
- [13] X. He, J. Chen, X. Ren, L. Zhang, Y. Liu, J. Feng, J. Fang, K. Zhao, S. Liu, *Adv. Mater.* **2021**, 33, 2100770.
- [14] D. Lübke, P. Hartnagel, J. Angona, T. Kirchartz, *Adv. Energy Mater.* **2021**, 11, 2101474.
- [15] O. Almora, D. Baran, G. C. Bazan, C. I. Cabrera, S. Erten-Ela, K. Forberich, F. Guo, J. Hauch, A. W. Y. Ho-Baillie, T. J. Jacobsson, R. A. J. Janssen, T. Kirchartz, N. Kopidakis, M. A. Loi, R. R. Lunt, X. Mathew, M. D. McGehee, J. Min, D. B. Mitzi, M. K. Nazeeruddin, J. Nelson, A. F. Nogueira, U. W. Paetzold, B. P. U. Rau, H. J. Snaith, E. Unger, L. Vaillant-Roca, C. Yang, H.-L. Yip, et al. *Adv. Energy Mater.* **2023**, 13, 2203313.
- [16] E. T. Hoke, D. J. Slotcavage, E. R. Dohner, A. R. Bowring, H. I. Karunadasa, M. D. McGehee, *Chem. Sci.* **2015**, 6, 613.
- [17] E. L. Unger, L. Kegelmann, K. Suchan, D. Sorell, L. Korte, S. Albrecht, *J. Mater. Chem. A* **2017**, 5, 11401.
- [18] S. Mahesh, J. M. Ball, R. D. Oliver, D. P. McMeekin, P. K. Nayak, M. B. Johnston, H. J. Snaith, *Energy Environ. Sci.* **2020**, 13, 258.
- [19] Z. Liu, J. Siekmann, B. Klingebiel, U. Rau, T. Kirchartz, *Adv. Energy Mater.* **2021**, 11, 2003386.
- [20] J. Tian, K. Zhang, Z. Xie, Z. Peng, J. Zhang, A. Osvet, L. Luer, T. Kirchartz, U. Rau, N. Li, C. J. Brabec, *ACS Energy Lett.* **2022**, 7, 4071.
- [21] H. Chen, A. Maxwell, C. Li, S. Teale, B. Chen, T. Zhu, E. Ugur, G. Harrison, L. Grater, J. Wang, Z. Wang, L. Zeng, S. M. Park, L. Chen, P. Serles, R. A. Awni, B. Subedi, X. Zheng, C. Xiao, N. J. Podraza, T. Filleter, C. Liu, Y. Yang, J. M. Luther, S. De Wolf, M. G. Kanatzidis, Y. Yan, E. H. Sargent, *Nature* **2022**, 613, 676.
- [22] M. Stolterfoht, P. Caprioglio, C. M. Wolff, J. A. Márquez, J. Nordmann, S. Zhang, D. Rothhardt, U. Hörmann, Y. Amir, A. Redinger, *Energy Environ. Sci.* **2019**, 12, 2778.
- [23] S. N. Agbo, T. Merdzhanova, U. Rau, O. Astakhov, *Sol. Energy Mater. Sol. Cells* **2017**, 159, 427.
- [24] F. Khan, S. N. Singh, M. Husain, *Sol. Energy Mater. Sol. Cells* **2010**, 94, 1473.
- [25] N. H. Reich, W. G. J. H. M. van Sark, E. A. Alsema, R. W. Lof, R. E. I. Schropp, W. C. Sinke, W. C. Turkenburg, *Sol. Energy Mater. Sol. Cells* **2009**, 93, 1471.
- [26] J. Merten, J. M. Asensi, C. Voz, A. V. Shah, R. Platz, J. Andreu, *IEEE Trans. Electron Devices* **1998**, 45, 423.
- [27] G. Burwell, O. J. Sandberg, W. Li, P. Meredith, M. Carnie, A. Armin, *Sol. RRL* **2022**, 6, 2200315.
- [28] R. Arai, S. Furukawa, Y. Hidaka, H. Komiyama, T. Yasuda, *ACS Appl. Mater. Interfaces* **2019**, 11, 9259.
- [29] R. Cheng, C.-C. Chung, H. Zhang, F. Liu, W.-T. Wang, Z. Zhou, S. Wang, A. B. Djurišić, S.-P. Feng, *Adv. Energy Mater.* **2019**, 9, 1901980.
- [30] J. Dagar, S. Castro-Hermosa, G. Lucarelli, F. Cacialli, T. M. Brown, *Nano Energy* **2018**, 49, 290.
- [31] C.-Y. Chen, J.-H. Chang, K.-M. Chiang, H.-L. Lin, S.-Y. Hsiao, H.-W. Lin, *Adv. Funct. Mater.* **2015**, 25, 7064.
- [32] L.-C. Kin, Z. Liu, O. Astakhov, S. Shcherbachenko, H. Kungl, T. Kirchartz, R.-A. Eichel, U. Rau, T. Merdzhanova, *Cell Rep. Phys. Sci.* **2022**, 3, 101123.
- [33] V. Bahrami-Yekta, T. Tiedje, *Opt. Express* **2018**, 26, 28238.
- [34] Z. Liu, L. Krückemeier, B. Krogmeier, B. Klingebiel, J. A. Márquez, S. Levchenko, S. Öz, S. Mathur, U. Rau, T. Unold, T. Kirchartz, *ACS Energy Lett.* **2019**, 4, 110.
- [35] M. A. Faist, S. Shoaee, S. M. Tuladhar, G. F. A. Dibb, S. Foster, W. Gong, T. Kirchartz, D. D. C. Bradley, J. R. Durrant, J. Nelson, *Adv. Energy Mater.* **2013**, 3, 744.
- [36] M. A. Faist, T. Kirchartz, W. Gong, R. S. Ashraf, I. McCulloch, J. C. de Mello, N. J. Ekins-Daues, D. D. C. Bradley, J. Nelson, *J. Am. Chem. Soc.* **2012**, 134, 685.
- [37] L. Krückemeier, Z. Liu, B. Krogmeier, U. Rau, T. Kirchartz, *Adv. Energy Mater.* **2021**, 11, 2102290.
- [38] M. A. Green, U. O. N. S. Wales, *Solar Cells: Operating Principles, Technology and System Applications*, University of New South Wales, Australia **1986**.

- [39] S. Hegedus, A. Luque, *Handbook of Photovoltaic Science and Engineering*, Wiley, USA **2011**.
- [40] M. A. Green, *Sol. Cells* **1982**, 7, 337.
- [41] S. Agbo, T. Merdzhanova, U. Rau, O. Astakhov, *Sol. Energy Mater. Sol. Cells* **2017**, 159, 427.
- [42] J. Merten, J. Asensi, C. Voz, A. Shah, R. Platz, J. Andreu, *IEEE Trans. Electron Devices* **1998**, 45, 423.
- [43] L. C. Hirst, N. J. Ekins-Daukes, *Prog. Photovoltaics* **2011**, 19, 286.
- [44] D. Grabowski, Z. Liu, G. Schöpe, U. Rau, T. Kirchartz, *Sol. RRL* **2022**, 6, 2200507.
- [45] D. Lübke, P. Hartnagel, M. Hülsbeck, T. Kirchartz, *ACS Mater. Au* **2023**, 3, 215.
- [46] M. Taguchi, A. Yano, S. Tohoda, K. Matsuyama, Y. Nakamura, T. Nishiwaki, K. Fujita, E. Maruyama, *IEEE J. Photovoltaics* **2014**, 4, 96.
- [47] S. K. Thomas, A. Pockett, K. Seunarine, M. Spence, D. Raptis, S. Meroni, T. Watson, M. Jones, M. J. Carnie, *IoT* **2022**, 3, 109.
- [48] X. Deng, X. Wen, J. Zheng, T. Young, C. F. J. Lau, J. Kim, M. Green, S. Huang, A. Ho-Baillie, *Nano Energy* **2018**, 46, 356.
- [49] S. Shao, M. Abdu-Aguye, L. Qiu, L.-H. Lai, J. Liu, S. Adjokatse, F. Jahani, M. E. Kamminga, H. Gert, T. T. Palstra, *Energy Environ. Sci.* **2016**, 9, 2444.